

Impact of aerosol optics on vertical distribution of ozone in autumn over YRD

Shuqi Yan², Bin Zhu^{1,*}, Shuangshuang Shi¹, Wen Lu¹, Jinhui Gao³, Hanqing Kang¹, Duanyang Liu²

¹Collaborative Innovation Center on Forecast and Evaluation of Meteorological Disasters, Key Laboratory for Aerosol-Cloud-Precipitation of China Meteorological Administration, Key Laboratory of Meteorological Disaster, Ministry of Education (KLME), Special Test Field of National Integrated Meteorological Observation, Nanjing University of Information Science & Technology, Nanjing 210044, China

²Key Laboratory of Transportation Meteorology of China Meteorological Administration, Nanjing Joint Institute for Atmospheric Sciences, Nanjing 210041, China

³Plateau Atmosphere and Environment Key Laboratory of Sichuan Province, School of Atmospheric Sciences, Chengdu University of Information Technology, Chengdu 610225, China

Correspondence to: Bin Zhu (binzhu@nuist.edu.cn)

Abstract. Tropospheric ozone, an important secondary pollutant, is greatly impacted by aerosols within boundary layer (BL). Previous studies have mainly attributed ozone variation to either aerosol-BL or aerosol-photolysis interactions at near surface. In this study, we analyze the sensitivities of ozone response to aerosol mixing states (e.g., mixing behavior hypothesis of scattering and absorbing components) in the vertical direction and address the effects of aerosol-BL and aerosol-photolysis interactions on ozone profiles in autumn by WRF-Chem simulations. The aerosol internal mixing state experiment reasonably reproduces the vertical distribution and time variation of meteorological elements and ozone. Sensitive experiments show that aerosols lead to turbulent suppression, precursor accumulation, lower-level photolysis reduction and upper-level photolysis enhancement. Consequently, ozone basically decreases within entire BL during daytime (08:00~17:00), and the decrease is the least in external mixing state (2.0%) compared with internal (10.5%) and core-shell mixing states (8.6%). The photolysis enhancement is the most significant in external mixing state due to its strong scattering ability. By process analysis, lower-level ozone chemical loss is enhanced due to photolysis reduction and NO_x accumulation under VOC-limited regime. Upper-level ozone chemical production is accelerated due to higher photolysis rate resulting from aerosol backscattering. Therefore, the increased ozone entrainment from aloft BL to surface induced by boosted ozone vertical gradient outweighs the decreased ozone entrainment induced by turbulent suppression after 11:00 am. Additional simulations support that aerosol effect on precursor, photolysis and ozone is consistent under different underlying surface and pollution conditions.

1 Introduction

Tropospheric ozone is an important secondary pollutant that is produced by the photochemistry of VOC (volatile organic

30 compounds) and NO_x . The variation of ozone is determined by the highly variable interactions among meteorology, precursors, photochemistry and aerosols. Tropospheric ozone, especially in the atmospheric boundary layer (BL), exerts side effects such as impairing human health, contributing to global warming and aggravating air pollution (Fu et al., 2019). Since 32 2013, the severe $\text{PM}_{2.5}$ pollution over East China has been mitigated but ozone concentration is increasing (Li et al., 2020). 33 Therefore, the characteristic of ozone variation and its relationship with external factors need to be intensively studied. 34

35 The interactions between ozone and aerosols are complicated and have attracted wide concern in recent years. Aerosols can significantly affect ozone photochemistry by influencing photolysis process (herein called aerosol-photolysis interaction). 36 The weakened solar radiation reaching the ground induced by aerosol extinction can decrease photolysis rate at the surface 37 and within several hundred meters above the surface, thus inhibiting ozone production and resulting in lower ozone concentration (Gao et al., 2020; Jacobson, 1998; Li et al., 2011). Contrarily, scattering aerosols increase upward shortwave radiation 38 which may promote ozone formation at a higher altitude (Gao et al., 2021a). Dickerson et al. (1997) and Shi et al. (2022) 39 demonstrated that aerosol pollution can remarkably increase ultraviolet radiation at a few hundred meters above the aerosol 40 layer, which accelerates photolysis and increase ozone concentration by about 3~20 ppb. Additionally, heterogeneous reactions 41 on aerosol surface can also influence ozone chemistry (Jacob, 2000; Li et al., 2019; Lou et al., 2014). 42 43

44 Aerosols affect BL thermodynamics and ultimately result in ozone change, which has attracted much attention in recent 45 years. The perturbation in radiation flux profile induced by aerosols can alter BL structure, thus influencing vertical mixing 46 and affecting ozone and precursor concentration (herein called aerosol-BL interaction). Aerosols stabilize BL and suppress 47 turbulent mixing (Ding et al., 2016; Li et al., 2017), which can inhibit the vertical exchange of ozone. Gao et al. (2018) studied 48 the effect of black carbon (BC) on ozone variation within BL. BC weakens turbulent mixing and inhibits the higher 49 ozone aloft being entrained downward. Additionally, the suppression of BL leads to the accumulation of NO_x which promotes 50 the formation of radicals and chemical production of ozone. The weakening in ozone mixing outweighs the enhancement 51 in ozone chemical production, so the surface ozone is decreased during the daytime.

52 The effect of aerosols on BL is related to aerosol optics, which are determined by aerosol morphology (Liu et al., 2019), hy-
53 groscopicity (Zeng et al., 2019), coating process (Bond et al., 2006) and chemical composition. The aerosol chemical com-
54 position in East China is dominated by SNA (sulfate, nitrate and ammonium) (larger than 50%), followed by organic matter
55 and BC (3~8%) (Yang et al., 2011; Tan et al., 2020, 2022). The contribution of SNA to total aerosol scattering coefficient can
56 reach up to 60% (Tian et al., 2015), and BC accounts for more than 70% of total aerosol absorbing coefficient (Yang et al.,
57 2008). Furthermore, aerosol optics are strongly affected by aerosol mixing states. Since the real-world mixing state is highly
58 variable and hard to be explicitly resolved (Riemer & West, 2013), three typical mixing states are generally hypothesized by
59 previous works: internal mixing, core-shell mixing and external mixing. The mixing state is largely affected by the mixing
60 behavior of BC with other aerosol species. The freshly emitted BC is commonly externally mixed with other species, but it

批注 [yansq1]:
Adding discussions about chemical
composition

61 ~~will become more internally mixed due to coating process (Riemer et al., 2019). The BC light absorption can be amplified by~~
62 ~~a factor of 50~200% after being coating with scattering aerosols (Cappa et al., 2012; Jacobson, 2001; Liu et al., 2017). The~~
63 ~~mixing behaviour hypothesis of aerosol scattering and absorbing components yields three major mixing states: internal mix-~~
64 ~~ing, core shell mixing and external mixing. In internal and core shell mixing, BC absorption can be enhanced by 50-100%~~
65 ~~(Bond et al., 2006; Jacobson, 2001). In external mixing, the absorption ability is weaker but scattering ability is stronger~~
66 ~~(Zeng et al., 2019).~~ Accordingly, aerosol mixing state alters aerosol optical properties and affects its interactions with BL and
67 photolysis. Gao et al. (2021b) found that aerosols result in smaller boundary layer height (PBLH) reduction in external mix-
68 ing (11.6 m) than in core-shell mixing (24 m), consequently leading to different changes in photolysis rates and ozone con-
69 centration.

70 Many studies reveal the aerosol effect on ozone at near-surface level. Aerosols notably affect ozone photochemistry at all
71 heights within BL and ultimately influence ozone vertical distribution and turbulent exchange. Therefore, the aero-
72 sol-induced ozone variation could have larger complexity and uncertainty in the vertical direction, which should be explored
73 further. Additionally, previous studies explain ozone variation mainly by either aerosol-BL or aerosol-photolysis interaction,
74 but relatively few of them consider these two mechanisms together. In this study, we aim to quantitatively reveal the impact
75 of aerosols on ozone profile through the two pathways (aerosol-BL and aerosol-photolysis interactions) by WRF-Chem sim-
76 ulations, as well as how aerosol effect varies with aerosol mixing states in autumn season over the Yangtze River Delta Re-
77 gion (YRD), China. Heterogeneous chemistry is not included in this study. The manuscript is organized as follows. Section 2
78 introduces the data, model and sensitive experiments. Section 3.1 evaluates the model performances. Sections 3.2 to 3.4 re-
79 veal the characteristic of aerosol-BL and aerosol-photolysis interactions and their impacts on ozone variation. Section 4 dis-
80 Discuss the robustness of simulation results under different conditions~~performs additional analysis and simulations to support~~
81 ~~the results~~. Section 5 concludes the findings of this study.

82 **2 Data, model and experiments**

83 **2.1 Data**

84 A field campaign was conducted at an industrial zone in north Nanjing suburban (118.71 °E, 32.27 °N) from 15 October to 15
85 November in November 2020 (Figure 1). We collected the vertical profiles of meteorological elements (temperature, wind
86 speed and direction) and air pollutants (PM_{2.5}, BC and ozone). Meteorological elements are measured by XLS-II tethered
87 balloon system with a sounding balloon at 08:00 and 14:00 local time. The data are sampled each second until it loses signal.
88 Air pollutants observation instruments are mounted on UAV platform. The UAV climbs vertically from the ground to about 1
89 km with a speed of 2m/s, and it descends along the same path at the same speed. The UAV is launched four times a day at

90 around 09:00, 11:00, 14:00 and 16:00 (local time). The introduction of observation instruments of PM_{2.5}, BC and ozone can
91 be referred to Shi et al. (2020, 2021). Meteorology and air pollutants profiles are averaged to 50 m intervals. These data are
92 used to evaluate the model performance in the vertical direction. ~~The model performance on meteorology and pollutants is~~
93 generally reasonable during the whole observation period. We mainly use the data from 2 to 5 November to study the effect
94 of aerosols on ozone, and detailly investigate the physical and chemical mechanisms in the pollution stage on 2 November.

95 The ground meteorology observation data is from MICAPS (Li et al., 2010), including temperature, wind speed and wind
96 direction that recorded every three hours. The ground air quality data is from China National Environmental Monitoring
97 Center (<https://www.aqistudy.cn/>), including PM_{2.5}, ozone and other pollutants. We use the temperature, wind speed, wind
98 direction, PM_{2.5} and ozone data to evaluate the model performance on the time series of meteorological elements and air
99 pollutants.

100 **2.2 Model configuration and sensitive experiments**

101 The model used in this study is the WRF-Chem (V3.9.1.1) model (Fast et al., 2006; Grell et al., 2005). It is the
102 state-of-the-art atmospheric model that online couples meteorology and chemistry. Two domains are set up with the central
103 point at the observation site (118.71 °E, 32.27 °N) (Figure 1). The parent domain has the size of 79×79 grids with the grid
104 spacing of 27 km. The inner domain has the size of 79×79 grids with the grid spacing of 9 km, covering the most part of the
105 Yangtze River Delta Region. To better describe the turbulent process, the vertical level is refined to 38 layers and 12 of
106 which are below 2 km. All the model results are calculated at the nearest grid close to the observation site if not specified.

107 The anthropogenic emission inventory in the base year of 2020 is provided by MEIC from Tsinghua University (Zheng et al.,
108 2018) (<http://www.meicmodel.org/>). MEIC includes major gaseous and aerosol species, e.g., SO₂, NH₃, VOCs, NO_x, BC,
109 PM_{2.5} and PM₁₀. The gas chemical mechanism is Carbon Bond Mechanism Z (CBMZ; Zaveri and Peters, 1999), and the
110 aerosol chemical mechanism is Model for Simulating Aerosol Interactions and Chemistry with four bins (MOSAIC-4bin;
111 Zaveri et al., 2008). These two chemical mechanisms are widely used for studying ozone chemistry. Detailed physical and
112 chemical schemes are listed in Table 1.

113 The initial and boundary fields of meteorology are provided by ERA5 0.25°×0.25° reanalysis data
114 (<https://cds.climate.copernicus.eu/cdsapp#!/dataset/reanalysis-era5-pressure-levels?tab=form>). The chemical initial and
115 boundary fields are provided by WACCM (<https://www2.acom.ucar.edu/gcm/waccm>). They are all updated every 6 hours.
116 The simulation starts at ~~08:00 on 30 October and ends at 20:00 on 2 November~~ 08:00 on 15 October and ends at 20:00 on 15
117 November, and the first 72h is spin-up period. All the time here is local time (UTC+8).

2.3 Aerosol optics and sensitive experiments

In this work, the effect of aerosol optics on ozone profiles is addressed by its mixing states. We study three ideal types of mixing states: internal mixing, core-shell mixing and external mixing, which depend on the mixing behavior hypothesis of scattering and absorbing components. In internal mixing state, the relative fractions of chemical species in one particle are the same as that of the bulk aerosols. The complex refractive index (RI) of bulk aerosols is calculated by the volume-averaged RI of all aerosol species, and then it is passed to Mie optical module to calculate the required optical parameters (e.g., scattering coefficient, absorbing coefficient and single scattering albedo). The detailed formulas of aerosol optical parameters for MOSAIC sectional scheme are documented by previous works (e.g., Fast et al., 2006; Grell et al., 2005). In core-shell mixing, aerosol particles are hypothesized to be concentric spheres with BC as the core and non-BC aerosols as the coating shell (Riemer et al., 2019). The RI of the shell is the volume-averaged RI of non-BC aerosols, and the optics of core-shell mixed particles can also be treated by the Mie optical module (Ackerman & Toon, 1981). In external mixing state, each particle contains only one species with fixed optical characteristics. It is not included in the current WRF-Chem model, and the approximate treatment has been proposed by Gao et al. (2021b). In general, the Mie optical module separates BC aerosols from the bulk aerosols, and treats the optics of non-BC and BC aerosols individually.

To study the aerosol effect on ozone, four experiments are conducted (Table 2). The case "int" is the base experiment (the default option in WRF-Chem), in which the aerosols are internally mixed. The cases "csm" and "ext" are core-shell mixing and external mixing, respectively. The case "noARI" turns off aerosol-radiation feedback by setting aerosol optical depth as zero in radiation and photolysis modules. Therefore, the difference between noARI and three other experiments indicates the effect of aerosols in the corresponding mixing state.

One should note that the real-world aerosol mixing state varies with emission, meteorology, composition, and other factors. The dynamic evolution of aerosol mixing state and its influencing factors have not been addressed in most current 3D models (Matsui et al., 2013). This work addresses aerosol optics by the three ideal mixing states, which will inevitably cause the simulated aerosol optics deviating from observation.

3 Results

[t] is an obvious pollution stage on 2 November 2020. The model evaluation on profiles (Section 3.1) and the mechanism of aerosols affecting ozone variation (Sections 3.2 to 3.4) are presented at the Nanjing site during that day. The model evaluation on time series (Section 3.1) and the aerosol effect under different pollution conditions (Section 4) are presented during the simulation period (15 October to 15 November).

批注 [yansq2]: Adding the definitions of mixing states and model limitations in this section.

批注 [yansq3]: Clearly state when to use the whole simulation period and when to use the single day of 2 Nov.

146 3.1 Model evaluations

147 ~~Four~~ additional sites around Nanjing, i.e., Changzhou (CZ), Huainan (HN), Maanshan (MS), and Huaian (HA) (Figure 1) are
148 chosen to evaluate the performance on the time variation of meteorological parameters (temperature, wind speed and wind
149 direction), PM_{2.5} and ozone in the base experiment (internal mixing). The statistical metrics include index of agreement
150 (IOA), mean bias (MB), root mean square error (RMSE), mean normalized bias (MNB) and mean fractional bias (MFB).
151 The calculations are from Lu et al. (1997), especially, the IOA of wind direction is from Kwok et al. (2010). Benchmark val-
152 ues of meteorology and air pollutants are derived from Emery et al. (2011) and EPA (2005; 2007). The temporal variations of
153 simulated meteorology and air pollutants are generally in good agreement with observations (Figure 2). From Table 3, tem-
154 perature presents the highest IOA, with a slightly large MB at HA site. The simulated wind direction is similar to observation,
155 and MB exceeds benchmark value at only one site. The simulated wind speed is a bit higher, which is because the WRF
156 model tends to overestimate wind speed due to the description of surface roughness (Jia and Zhang, 2020, 2021; Jim énez and
157 Dudhia, 2012). PM_{2.5} is moderately overestimated, but all the metrics are within the benchmarks. The IOA of ozone exceeds
158 0.8 at all sites, and only one site shows a MNB out of benchmark. The model statistical metrics of PM_{2.5} and ozone are con-
159 sistent with previous works (Chen et al., 2022; Hu et al., 2016; Singh et al., 2012; Zhang et al., 2014a). Generally, the base
160 experiment simulations on the temporal variation of meteorology and air pollutants are acceptable, which reasonably repro-
161 duces the observations in the atmosphere.

162 ~~It is an obvious pollution stage on 2 November 2020 (Figure 2). We mainly evaluate the simulated profiles on that day. Fig-~~
163 ~~ure 3~~ Figure 3 shows the model performance of meteorological parameters (temperature, wind speed and wind direction) and
164 air pollutants (ozone, PM_{2.5} and BC). Seen from the profiles, temperature shows a similar pattern between simulation and
165 observation, with the mean bias of 0.7 K and the maximum bias of 1.7-6K. The simulated wind direction and wind speed
166 agree well with observation, except that wind speed is overestimated for 1.2~1.9 m/s at 14:00. ~~Comparing the observed and~~
167 ~~simulated time series at near surface, temperature variation is successfully reproduced, with the maximum bias of about~~
168 ~~1.5 K. Wind speed is overestimated for about 2m/s at 16:00 and 17:00. The base experiment reasonably simulates meteoro-~~
169 ~~logical parameters, which provides the basis for the satisfying simulation of air pollutants.~~ The ozone profile shows ac-
170 ceptable performance, with the concentration being underestimated for about 2~12 ppb at 14:00 and 16:00. The simulated
171 PM_{2.5} profile is generally consistent with observations. There is a moderate underestimation of 40~6080 µg/m³ at 11:00 be-
172 low 800 m ~~and a slight overestimation of about 10-20 µg/m³ at 14:00~~. BC profile is almost close to observation, with the
173 maximum bias of about 2~3 µg/m³. Overall, the model reasonably captures the vertical structure and temporal variation of
174 meteorological elements, PM_{2.5}, BC and ozone, which is crucial for exploring the mechanism of aerosol-BL and aéro-
175 sol-photolysis interactions and explaining their impacts on ozone vertical profile.

批注 [yansq4]: A newly added para-
graph: model evaluation at more sites

批注 [yansq5]: Section titles are revised to convey the meanings more clearly

3.2 Impact of ~~aerosol-BL interactions~~ aerosols on BL and NO_x

The effects of aerosols are detailly studied at the Nanjing site on 2 November 2020. Figure 4a shows the effect of aerosols on PBLH. Aerosols consistently decrease PBLH in all mixing states, with the reduction of ~~178m-152m~~ (48.515.5%), ~~201m-174m~~ (20.917.8%) and ~~156m-136m~~ (46.314.0%) in internal, core-shell and external mixing conditions, respectively. External mixing exerts the weakest PBLH reduction effect here, which is also reported by Gao et al. (2021b). The mechanism of BL suppression by aerosols has been elucidated by many studies (e.g., Ding et al., 2016; Li et al., 2017). The suppression of BL can inhibit turbulent exchange (Figure 4b) and favour the accumulation of precursor contents near the surface. NO_x generally increases at all heights within BL (Figure 4c), and this increase is significantly larger at lower heights than at upper heights. At near surface, the increase is about ~~4-2~~ ppb for internal and core-shell mixing and about ~~2-1~~ ppb for external mixing.

The change in NO_x may alter the ozone chemical regime and influence the sensitivity of ozone to VOC and NO_x. In this study, ozone chemical regime is indicated by $R=H_2O_2/HNO_3$. For Yangtze-River-Delta Region, ozone chemistry is in NO_x-limited regime if $R>0.8$ or in VOC-limited regime if $R<0.6$ or in transition regime if $0.6<R<0.8$ (Qu et al., 2021). The differences in R are small among various aerosol mixing states (Figure 5). Below the height of about ~~300m-400m~~, ozone is NO_x-limited during 08:00~10:00 and VOC-limited after 10:00. While at the heights above ~~300m-400m~~, ozone is dominantly VOC-limited in the whole daytime of 2 November. It indicates that despite the change in precursor concentrations, ozone chemical regime almost remains unchanged and it is mainly controlled by VOC. Therefore, the increase in NO_x can enhance NO titration effect and inhibit ozone production, which will be further discussed in Section 3.4. Statistics on the entire model region also show that ozone chemical regime remains unchanged in most areas (>95%) and the dominant type is VOC-limited regime (>92%). Such is the case in the areas with urban or rural surfaces, and in the areas with high or low NO_x emission rates.

3.3 Impact of ~~aerosol-photolysis interactions~~ aerosols on photolysis

The photolysis of NO₂ (JNO₂) and ozone (JO1D) are two major reactions that contribute to ozone production. In noARI condition, photolysis rates increase with height due to atmospheric extinction (figure not shown). When aerosol effect is included, photolysis rates decrease sharply at lower level but increase at upper level in all mixing states (Figure 6a and b). At the surface level, the relative change of JNO₂ and JO1D in internal mixing state is approximately -30%, which is similar to the value of -22.6% reported by Wu et al. (2020) and -23.0% by Zhao et al. (2021) that conducted in autumn and winter seasons. Notably, in external mixing state, the lower-level decrease is the smallest and the upper-level increase is the largest, with the maximum increase of about ~~exceeding~~ 10%. Also, the height where photolysis rate (e.g., JNO₂) starts to increase is lower in external mixing state (~~~500m-700m~~) than in other mixing states (~~~1000m-1200m~~).

206 The significant differences in photolysis change can be explained by aerosol optical properties and its impact on radiation
207 transfer. The aerosol extinction coefficient shows no obvious differences under the three mixing states, with the maximum
208 difference of about 0.05 km^{-1} (Figure 6c). However, the single scatter albedo (SSA) shows distinct differences (Figure 6d).
209 SSA is about 0.8~0.9 in internal and core-shell mixing conditions below 2000m, and it is about 0.90~0.98 in external mixing
210 condition which indicates a strong scattering ability. Zeng et al. (2019) also found that SSA is the largest in external mixing
211 state compared with other mixing states. Therefore, it will backscatter more solar radiation to the upper level (Figure 6e) and
212 promotes photolysis there (Figure 6a and b). Shi et al. (2022) have provided observational evidence that aerosols can in-
213 crease upwelling shortwave radiation and promote photolysis at the upper level.

214 3.4 Impact of aerosol-BL and aerosol-photolysis interactions aerosols on ozone profile

215 Figure 7 shows the ozone profile in various mixing states. We focus on the ozone within BL in the daytime. During
216 08:00~11:00, the BL is in increasing stage, and ozone increases with height within BL. The average changes in ozone under
217 internal, core-shell and external mixing are $-10.39.7$ ppb ($-17.15.8\%$), $-8.78.5$ ppb ($-14.513.8\%$) and $-3.73.3$ ppb ($-6.15.4\%$),
218 respectively. As BL develops during 11:00~17:00, ozone shows a strong a-positive gradient near the surface, uniform distri-
219 bution above the surface and negative gradient at upper BL. The average change in ozone under internal, core-shell and ex-
220 ternal mixing is $-6.27.3$ ppb ($-8.19.3\%$), $-4.45.9$ ppb ($-5.97.5\%$) and $+0.5-1.0$ ppb ($+0.7-1.2\%$), respectively. During the day-
221 time (08:00~17:00), ozone reduction is larger in internal ($9.810.5\%$) and core-shell mixing states ($7.48.6\%$) and the smallest
222 in external mixing state ($0.62.0\%$). The reduction (about 3~13%) is the largest at near surface, which is due to that the NO_x
223 accumulation and photolysis inhibition are more profound at near surface. Other studies also reveal that ozone reductions
224 caused by aerosols are approximately in the range of 10~20% (e.g., Gao et al., 2020; Qu et al., 2021; Yang et al., 2022).
225 Above surface where the layer is more well-mixed, ozone reduction is relatively weaker. It can be inferred that diurnal ozone
226 concentration is generally reduced in all mixing states and at all heights within BL. The reduction is the smallest in external
227 mixing state, and the ozone below about 1000m shows a slight increase after 11:00 (Figure 7b). It could be because the en-
228 hanced NO titration effect associated with NO_x accumulation is weaker in external mixing than in other mixing states
229 (Figure 4c). Also, externally mixed aerosols lead to less photolysis suppression in the lower level and larger photolysis en-
230 hancement in the upper level (Figure 6a and b), which will partly counteract the reduction in ozone concentration.

231 To illustrate the mechanism of aerosols affecting ozone variation, we perform process analysis on ozone (Zhang et al.,
232 2014b). In this study, ozone is decomposed into vertical mixing (VMIX), net chemical production (CHEM) and advection
233 (ADVC; including horizontal and vertical advection) (Figure 8). The sign of CHEM depends on the competition between
234 ozone production and loss. Under the effect of aerosols, CHEM shows negative change at near surface and positive change
235 from lower to upper BL (Figure 8f-h). The negative CHEM change can be explained by the decrease in photolysis rate
236 (Figure 6a and b) and the increase in NO titration associated with NO_x accumulation (Figure 4c). Photolysis reduction may

批注 [y6]: Adding some more descriptions about ozone variation

237 inhibit ozone production, and the increased NO titration consumes more ozone under VOC-limited regime (Figure 5f). From
238 lower to upper BL, the positive CHEM change is dominantly contributed by the significant photolysis enhancement (Figure
239 6a and b). Since photolysis enhancement is the strongest in external mixing state, the increase in CHEM is the largest com-
240 pared with other mixing states (Figure 8f-h). Above BL, especially between the solid and dash lines, the change in CHEM is
241 negative due to the inhibited turbulent transport of NO_x from the BL.

242 The variation in ozone photochemistry indicated by CHEM can influence VMIX which depends on ozone vertical gradient
243 and turbulent exchange. In noARI condition, VMIX presents three distinct entrainment zones according to its signs: positive
244 zone near the surface, negative zone at lower-to-middle BL, and time-variant zone at upper BL (near PBLH). VMIX is posi-
245 tive near the surface and negative at lower-to-middle BL (Figure 8a), because the higher concentration of ozone aloft is en-
246 trained downward by turbulent mixing. The time-variant VMIX zone at upper BL, specifically, negative values during
247 08:00~11:00 and positive values during 11:00~16:00 (Figure 8a), is determined by the relationship between PBLH diurnal
248 variation and ozone vertical gradient below PBLH. During 08:00~11:00, ozone gradient at upper BL is positive (Figure 7a),
249 which causes entrainment loss at that height. Above BL where ozone gradient and turbulent mixing are weak, ozone vertical
250 exchange is not significant. Consequently, VMIX is negative at upper BL. During 11:00~16:00, ozone gradient at upper BL
251 is negative (Figure 7b), which causes entrainment gain at that height and the positive VMIX at upper BL. Under the effect of
252 aerosols, VMIX notably increases near the surface and basically decreases above surface in all mixing states especially after
253 11:00 (Figure 8b-d). It is because that the reinforced NO titration effect near surface and the enhanced photolysis aloft
254 strengthen the ozone vertical gradient. The increase in gradient promotes ozone vertical exchange, compensating for the
255 weakened ozone entrainment due to turbulent suppression, and instead, more ozone aloft are entrained to near surface (Gao
256 et al., 2020, 2021a). At upper BL, the change in VMIX is negative during 08:00~11:00 and positive during 11:00~16:00. It is
257 possibly due to that the negative and positive VMIX zones in Figure 8a move downward as PBLH decreases. The change in
258 ADVC is generally positive (Figure 8j-l), and its contribution of ADVC is relatively not important compared with VMIX and
259 CHEM.

260 ~~[Table 4] quantitatively describes the respective contributions of three processes to ozone variation during 11:00–17:00. From~~
261 ~~near surface to lower BL (0–300m), the positive VMIX contribution is stronger than the negative CHEM contribution, and~~
262 ~~the role of ADVC can be ignored. At lower to middle BL (300–800m), the promoting effect of VMIX on ozone weakens,~~
263 ~~and instead, the negative contribution of CHEM turns to positive and becomes the dominant influencing factor. At the upper~~
264 ~~BL (800–1500m), VMIX plays the dominant role due to the increasing ozone entrainment at upper BL (Figure 8b-d). The~~
265 ~~relative contributions of the three processes are generally consistent in all mixing states.~~

批注 [y7]: The original Table4 and its discussions are deleted.

266 **4 Discussions**

267 Above we have presented the variation in photolysis rates, ozone precursors and ozone concentration induced by aerosols in
268 a polluted day. To make the results more convincing, we perform additional analysis and simulations. The effect of aerosols
269 on ozone may depend on locations and the underlying surface type, e.g., urban and rural surfaces (Zhu et al., 2015). From
270 Table 4, the qualitative results are consistent among different sites and underlying surfaces~~differences between urban and~~
271 ~~rural are not obvious~~. Ozone shows a consistent decreasing and NO_x shows a consistent increasing feature under the effect of
272 aerosols. Photolysis rate (e.g., JNO₂) basically presents the dual change (i.e., lower-level decreasing and upper-level increas-
273 ing). Comparing the three mixing types, the changes in photolysis rates, ozone precursors and ozone concentration caused by
274 externally mixed aerosols are most favourable for mitigating ozone reduction. The mechanisms have been explained in pre-
275 vious sections.

276 The ozone variations during representative clean and polluted episodes are shown in Table 5. The ozone concentrations
277 within BL in internal mixing experiment are consistently reduced during all episodes. The core-shell mixing state shows
278 slightly lower reductions than internal mixing, and the ozone reductions are the least in external mixing state. The differences
279 in ozone relative changes between clean and polluted episodes are distinct. For example, in the internal mixing state, the rel-
280 ative reductions are about 0~5% in clean episodes and 6~11% in polluted episodes, indicating that the aerosol effect is more
281 profound under high aerosol contents. On 2 November which is the highest pollution episode during the study period, the
282 relative changes of ozone are approximately -11~-2% in three mixing states. It can be inferred that aerosol effect on photoly-
283 sis rates, ozone precursors and ozone concentration might be consistent under different underlying surface and pollution
284 conditions, and it is more significant in high aerosol conditions.

285 ~~We extend the simulations for 3 days (2 November 20:00 to 5 November 20:00) to examine the aerosol effect under different~~
286 ~~pollution conditions (Figure 9). The extended periods are relatively clean conditions, with the average PM_{2.5} being about 1/3~~
287 ~~of 2 November. In this clean episode, the NO_x variation also shows the same pattern as Figure 4. Photolysis rate still exhibits~~
288 ~~dual changes in external mixing state, while it decreases at all heights in internal and core shell mixing states. Ozone con-~~
289 ~~centration is also reduced and the reduction is the smallest in external mixing condition. Due to the relatively low aerosol~~
290 ~~content during this period, the changes in these quantities are much weaker than those during the pollution episode (2 No-~~
291 ~~vember). It can be inferred that aerosol effect on photolysis rates, ozone precursors and ozone concentration might be con-~~
292 ~~sistent under different underlying surface and pollution conditions, and it is more significant in polluted conditions.~~

域代码已更改

批注 [yansq8]: A newly added para-
graph, replacing the following deleted
paragraph.

293 5 Conclusions

294 Previous studies mainly focus on the relationship between aerosols and ozone at near surface and attribute ozone variation to
295 either aerosol-BL or aerosol-photolysis interactions. In this work, we explore the sensitivities of ozone response to aerosol
296 mixing states in the vertical direction by WRF-Chem simulations ~~during an air pollution case from 15 October to 15 2 to 5~~
297 November 2020 ~~in Nanjing over the Yangtze River Delta Region~~. Generally, the model reasonably captures the vertical pro-
298 files and temporal variation of meteorological elements, ozone, PM_{2.5} and BC. Sensitive experiments show that:

299 Aerosols influence ozone vertical variation through aerosol-BL and aerosol-photolysis interactions. Aerosol inhibits BL de-
300 velopment, resulting in more NO_x accumulated within BL and a stronger NO titration effect under VOC limited regime. The
301 PBLH reduction and NO_x accumulation are the smallest in external mixing state. Despite the change in precursor concentra-
302 tion, ozone chemical regime is still dominantly controlled by VOC (>95%) under different underlying surface and emission
303 conditions. Aerosols inhibit photolysis at lower level (~30%) but enhance photolysis at upper level (~10%) due to aerosol
304 backscattering. The enhanced photolysis is more obvious in external mixing state owing to its strong scattering ability.

305 Aerosols basically lead to ozone reduction (0.2~10%) at all heights within BL during the daytime (08:00~17:00), with the
306 least reduction (0.52.0%) ~~and a slight increase (0.7%)~~ in external mixing state ~~after 11:00~~. Such ozone variation is attributed
307 to the changes in VMIX, CHEM and ADV. CHEM decreases at near surface due to photolysis reduction and NO_x accumu-
308 lation, but increases from lower to upper BL due to photolysis enhancement. The photolysis reduction and NO_x accumulation
309 at lower level lead to ozone depletion and stronger vertical gradient, which promotes higher concentration of ozone aloft
310 being entrained downward. Therefore, VMIX increases at near surface but decreases at lower-to-middle BL. VMIX variation
311 at upper BL (near PBLH) is complex, which is determined by the relationship between PBLH diurnal variation and ozone
312 gradient near PBLH. ~~Quantitative comparisons among these processes show that: From near surface to lower BL (0-300m),~~
313 ~~positive VMIX contribution outweighs the negative CHEM contributions. At lower to middle BL (300-800m), positive~~
314 ~~VMIX contribution decreases, and CHEM becomes the dominant positive contributor. At upper BL (800-1500m), VMIX~~
315 ~~plays the dominant role.~~ Additional analysis indicate that aerosols could consistently cause precursor accumulation, dual
316 change of photolysis and ozone reduction under different underlying surface and pollution conditions.

317
318 *Code and data availability.* Some of the data repositories have been listed in Section 2. The other data, model outputs and
319 codes can be accessed by contacting Bin Zhu via binzhu@nuist.edu.cn.

320 *Author contributions.* SY performed the model simulation, data analysis and manuscript writing. BZ proposed the idea, su-
321 pervised this work and revised the manuscript. SS provided the data at observation site. WL, JG and HK offered helps to the

批注 [y9]: The original Table 4 and corresponding discussions are removed.

322 model simulation. DL helped the revision of the manuscript.

323 *Competing interests.* The authors declare that they have no conflict of interest.

324 *Acknowledgements.* This work is supported by the National Natural Science Foundation of China (Grant Nos. 92044302,
325 42192512 and 42275115).

326

327 **References**

- 328 Ackerman, T. P. and Toon, O. B.: Absorption of visible radiation in atmosphere containing mixtures of absorbing and
329 non-absorbing particles, *Appl. Optics*, 20, 3661–3662, <https://doi.org/10.1364/AO.21.000758>, 1981.
- 330 Bond, T. C., Habib, G., and Bergstrom, R. W.: Limitations in the enhancement of visible light absorption due to mixing state,
331 *J. Geophys. Res.*, 111, 360, <https://doi.org/10.1029/2006JD007315>, 2006.
- 332 Chen, Y., Fung, J. C., Huang, Y., Lu, X., Wang, Z., Louie, P. K., & Lau, A. K.: Temporal source apportionment of PM_{2.5} over
333 the Pearl River Delta region in southern China, *J. Geophys. Res.-Atmos.*, 127(14), e2021JD035271,
334 <https://doi.org/10.1029/2021JD035271>, 2022.
- 335 Dickerson, R. R., Kondragunta, S., Stenchikov, G., Civerolo, K. L., Doddridge, B. G., and Holben, B. N.: The impact of aer-
336 osols on solar ultraviolet radiation and photochemical smog, *Science*, 278, 827–830,
337 <https://doi.org/10.1126/science.278.5339.827>, 1997.
- 338 Ding, A. J., Huang, X., Nie, W., Sun, J. N., Kerminen, V. M., Petaja, T., Su, H., Cheng, Y. F., Yang, X. Q., Wang, M. H., Chi,
339 X. G., Wang, J. P., Virkkula, A., Guo, W. D., Yuan, J., Wang, S. Y., Zhang, R. J., Wu, Y. F., Song, Y., Zhu, T., Zilitink-
340 evich, S., Kulmala, M., and Fu, C. B.: Enhanced haze pollution by black carbon in megacities in China, *Geophys. Res.*
341 *Let.*, 43, 2873–2879, <https://doi.org/10.1002/2016GL067745>, 2016.
- 342 EPA, U.S.: Guidance on the Use of Models and Other Analyses in Attainment Demonstrations for the 8-hour Ozone NAAQS,
343 EPA-54/R-05-002, 2005.
- 344 EPA, U.S.: Guidance on the Use of Models and Other Analyses or Demonstrating Attainment of Air Quality Goals for Ozone,
345 PM_{2.5}, and Regional Haze, EPA-454/B-07-002, 2007.
- 346 Fast, J. D., Gustafson, W. I., Easter, R. C., Zaveri, R. A., Barnard, J. C., Chapman, E. G., Grell, G. A., and Peckham, S. E.:
347 Evolution of ozone, particulates, and aerosol direct radiative forcing in the vicinity of Houston using a fully coupled
348 meteorology-chemistry-aerosol model, *J. Geophys. Res.*, 111, <https://doi.org/10.1029/2005jd006721>, 2006.
- 349 Fierce, L., Bond, T., Bauer, S., et al. Black carbon absorption at the global scale is affected by particle-scale diversity in
350 composition. *Nat Commun*, 7, 12361, <https://doi.org/10.1038/ncomms12361>, 2016.
- 351 Fu, Y., Liao, H., & Yang, Y.: Interannual and decadal changes in tropospheric ozone in China and the associated chemistry-
352 climate interactions: A review, *Adv. Atmos. Sci.*, 36(9), 975–993, <https://doi.org/10.1007/s00376-019-8216-9>, 2019.
- 353 Gao, J., Zhu, B., Xiao, H., Kang, H., and Pan, C.: Effects of black carbon and boundary layer interaction on surface ozone in
354 Nanjing, China, *Atmos. Chem. Phys.*, 18, 7081–7094, <https://doi.org/10.5194/acp-2017-1177>, 2018.

355 Gao, J., Li, Y., Zhu, B., Hu, B., Wang, L., and Bao, F.: What have we missed when studying the impact of aerosols on surface
356 ozone via changing photolysis rates?, *Atmos. Chem. Phys.*, 20, 10831–10844,
357 <https://doi.org/10.5194/acp-20-10831-2020>, 2020.

358 Gao, J., Li, Y., Xie, Z., Wang, L., Hu, B., and Bao, F.: Do Absorbing Aerosols or Scattering Aerosols Dominate the Impact of
359 Aerosols on Ozone via Influencing Photolysis Rates?, *Earth and Space Science Open Archive*,
360 <https://doi.org/10.1002/essoar.10508565.1>, 2021a.

361 Gao, M., Yang, Y., Liao, H., Zhu, B., Zhang, Y., Liu, Z., Lu, X., Wang, C., Zhou, Q., Wang, Y., Zhang, Q., Carmichael, G. R.,
362 and Hu, J.: Reduced light absorption of black carbon (BC) and its influence on BC-boundary-layer interactions during
363 “APEC Blue”, *Atmos. Chem. Phys.*, 21, 11405–11421, <https://doi.org/10.5194/acp-21-11405-2021>, 2021b.

364 Grell, G. A., Peckham, S. E., Schmitz, R., McKeen, S. A., Frost, G., Skamarock, W. C., and Eder, B.: Fully coupled “online”
365 chemistry within the WRF model, *Atmos. Environ.*, 39, 6957–6975, <https://doi.org/10.1016/j.atmosenv.2005.04.027>,
366 2005.

367 Hu, J., Chen, J., Ying, Q., & Zhang, H. One-year simulation of ozone and particulate matter in China using WRF/CMAQ
368 modeling system, *Atmos. Chem. Phys.*, 16(16), 10333-10350, <https://doi.org/10.5194/acp-16-10333-2016>, 2016.

369 Jacob, D. J.: Heterogeneous chemistry and tropospheric ozone, *Atmospheric Environ.*, 34, 2131-2159,
370 [https://doi.org/10.1016/S1352-2310\(99\)00462-8](https://doi.org/10.1016/S1352-2310(99)00462-8), 2000.

371 Jacobson, M. Z. Studying the effects of aerosols on vertical photolysis rate coefficient and temperature profiles over an urban
372 airshed, *J. Geophys. Res.: Atmos.*, 103(D9), 10593, <https://doi.org/10.1029/98JD00287>, 1998.

373 Jacobson, M. Z.: Strong radiative heating due to the mixing state of black carbon in atmospheric aerosols, *Nature*,
374 <https://doi.org/10.1038/35055518>, 2001.

375 Jia, W., & Zhang, X. The role of the planetary boundary layer parameterization schemes on the meteorological and aerosol
376 pollution simulations: a review. *Atmos. Res.*, 239, 104890, <https://doi.org/10.1016/j.atmosres.2020.104890>, 2020.

377 Jia, W., & Zhang, X. Impact of modified turbulent diffusion of PM_{2.5} aerosol in WRF-Chem simulations in eastern China.
378 *Atmos. Chem. Phys.*, 21(22), 16827-16841, <https://doi.org/10.5194/acp-2021-435>, 2021.

379 Jiménez, P. A. and Dudhia, J.: Improving the representation of resolved and unresolved topographic effects on surface wind
380 in the WRF model, *J. Appl. Meteorol. Climatol.*, 51, 300–316, <https://doi.org/10.1175/JAMC-D-11-084.1>, 2012.

381 Kwok, R. H. F., Fung, J. C. H., Lau, A. K. H., and Fu, J. S.: Numerical study on seasonal variations of gaseous pollutants and
382 particulate matters in Hong Kong and Pearl River Delta Region, *J. Geophys. Res.*, 115, D16308,
383 <https://doi.org/10.1029/2009JD012809>, 2010.

384 Li, J., Wang, Z., Wang, X., Yamaji, K., Takigawa, M., Kanaya, Y.: Impacts of aerosols on summertime tropospheric photoly-
385 sis frequencies and photochemistry over central eastern china, *Atmos. Environ.*, 45(10), 1817-1829,
386 <https://doi.org/10.1016/j.atmosenv.2011.01.016>, 2011.

387 Li, K., Jacob, D. J., Liao, H., Zhu, J., Shah, V., Shen, L., Bates, K., Zhang, Q., & Zhai, S.: A two-pollutant strategy for im-
388 proving ozone and particulate matter air quality in China, *Nat. Geosci.*, 12, 906-910,
389 <https://doi.org/10.1038/s41561-019-0464-x>, 2019.

390 Li, K., Jacob, D. J., Shen, L., Lu, X., de Smedt, I., & Liao, H.: Increases in surface ozone pollution in China from 2013 to
391 2019: anthropogenic and meteorological influences, *Atmos. Chem. Phys.*, 20, 11423-11433,
392 <https://doi.org/10.5194/acp-20-11423-2020>, 2020.

393 Li, Y., Cao, L., Gao, S., and Luo, B.: The Current Stage and Development of MICAPS, *Meteorological Monthly*, 36, 50–55,

394 2010 (in Chinese).

395 Li, Z. Q., Guo, J. P., Ding, A. J., Liao, H., Liu, J. J., Sun, Y. L., Wang, T. J., Xue, H. W., Zhang, H. S., and Zhu, B.: Aerosol
396 and boundary-layer interactions and impact on air quality, *Natl. Sci. Rev.*, 4, 810–833,
397 <https://doi.org/10.1093/nsr/nwx117>, 2017.

398 Liu, C., Xu, X., Yin, Y., Schnaiter, M., & Yung, Y. L. Black carbon aggregates: A database for optical properties, *J Quant*
399 *Spectrosc Radiat Transf*, 222, 170-179, <https://doi.org/10.1016/j.jqsrt.2018.10.021>, 2019.

400 Liu, D., Whitehead, J., Alfarra, M. R., Reyes-Villegas, E., Spracklen, D. V., Reddington, C. L., & Allan, J. D.: Black-carbon
401 absorption enhancement in the atmosphere determined by particle mixing state, *Nat. Geosci.*, 10(3), 184-188,
402 <https://doi.org/10.1038/ngeo2901>, 2017.

403 Lou, S., Liao, H., & Zhu, B.: Impacts of aerosols on surface-layer ozone concentrations in China through heterogeneous re-
404 actions and changes in photolysis rates, *Atmos. Environ.*, 85, 123-138, doi:10.1016/j.atmosenv.2013.12.004, 2014.

405 Lu, R., Turco, R. P., and Jacobson, M. Z.: An integrated pollution modeling system for urban and regional scales: 2. Simula-
406 tions for SCAQS 1987, *J. Geophys. Res.*, 102, 6081–6098, <https://doi.org/10.1029/96JD03502>, 1997.

407 Matsui, H., Koike, M., Kondo, Y., Moteki, N., Fast, J. D., and Zaveri, R. A.: Development and validation of a black carbon
408 mixing state resolved three-dimensional model: Aging processes and radiative impact, *J. Geophys. Res.-Atmos.*, 118,
409 2304–2326, <https://doi.org/10.1029/2012JD018446>, 2013.

410 Qu, Y., Voulgarakis, A., Wang, T., Kasoar, M., Wells, C., Yuan, C., Varma, S., and Mansfield, L.: A study of the effect of aer-
411 osols on surface ozone through meteorology feedbacks over China, *Atmos. Chem. Phys.*, 21, 5705–5718,
412 <https://doi.org/10.5194/acp-21-5705-2021>, 2021.

413 Riemer, N., & West, M. Quantifying aerosol mixing state with entropy and diversity measures. *Atmos. Chem. Phys.*, 13(22),
414 11423–11439, <https://doi.org/10.5194/acp-13-11423-2013>, 2013.

415 Riemer, N., Ault, A. P., West, M., Craig, R. L., & Curtis, J. H. Aerosol mixing state: Measurements, modeling, and impacts.
416 *Rev. Geophys.*, 57, 187–249. <https://doi.org/10.1029/2018RG000615>, 2019.

417 Shi, S., Zhu, B., Lu, W., Yan, S., Fang, C., Liu, H., Liu, D., Liu, C.: Estimation of radiative forcing and heating rate based on
418 vertical observation of black carbon in Nanjing, China, *Sci. Tot. Environ.*,
419 <https://doi.org/10.1016/j.scitotenv.2020.144135>, 2020.

420 Shi, S., Zhu, B., Tang, G., Liu, C., An, J., Liu, D., Xu, J., Xu, H., Liao, H., & Zhang, Y.: Observational evidence of aerosol
421 radiation modifying photochemical ozone profiles in the lower troposphere, *Geophys. Res. Lett.*, 49, e2022GL099274,
422 <https://doi.org/10.1029/2022GL099274>, 2022.

423 Singh, H. B., Cai, C., Kaduwela, A., Weinheimer, A., & Wisthaler, A. Interactions of fire emissions and urban pollution over
424 California: Ozone formation and air quality simulations, *Atmos. Environ.*, 56, 45-51,
425 <https://doi.org/10.1016/j.atmosenv.2012.03.046>, 2012.

426 Tan, Y., Wang, H., Shi, S., Shen, L., Zhang, C., Zhu, B., & Liu, A.: Annual variations of black carbon over the Yang-tze Riv-
427 er Delta from 2015 to 2018, *J. Environ.l Sci.*, 96, 72-84, <https://doi.org/10.1016/j.jes.2020.04.019>, 2020.

428 Tan, Y., Wang, H., Zhu, B., Zhao, T., Shi, S., Liu, A., & Cao, L.: The interaction between black carbon and plane-tary
429 boundary layer in the Yangtze River Delta from 2015 to 2020: Why O₃ didn't decline so significantly as PM_{2.5}, *Environ.*
430 *Res.*, 214, 114095, <https://doi.org/10.1016/j.envres.2022.114095>, 2022.

431 Tian, P., Wang, G., Zhang, R., Wu, Y., & Yan, P.: Impacts of aerosol chemical compositions on optical properties in urban
432 Beijing, China, *Particuology*, 18, 155-164., <https://doi.org/10.1016/j.partic.2014.03.014>, 2015.

433 Wu, J., Bei, N., Hu, B., Liu, S., Wang, Y., Shen, Z., Li, X., Liu, L., Wang, R., Liu, Z., Cao, J., Tie, X., Molina, L. T., and Li,
434 G.: Aerosol-photolysis interaction reduces particulate matter during wintertime haze events, *Proc. Natl. Acad. Sci. USA*,
435 117, 9755–9761, <https://doi.org/10.1073/pnas.1916775117>, 2020.

436 Yang, F., Tan, J., Zhao, Q., Du, Z., He, K., Ma, Y., & Chen, G.: Characteristics of PM_{2.5} speciation in repre-sentative megaci-
437 ties and across China, *Atmos. Chem. Phys.*, 11(11), 5207-5219, <https://doi.org/10.5194/acpd-11-1025-2011>, 2011.

438 Yang, H., Chen, L., Liao, H., Zhu, J., Li, X.: Impacts of aerosol-photolysis interaction and aerosol-radiation feedback on
439 surface-layer ozone in north china during a multi-pollutant air pollution episode, *Atmos. Chem. Phys.*, 22(6), 4101–4116,
440 <https://doi.org/10.5194/acp-2021-1192022>, 2022.

441 Yang, M., Howell, S. G., Zhuang, J., and Huebert, B. J.: Attribution of aerosol light absorption to black carbon, brown
442 car-bon, and dust in China – interpretations of atmospheric measurements during EAST-AIRE, *Atmos. Chem. Phys.*, 9,
443 2035–2050, <https://doi.org/10.5194/acp-9-2035-2009>, 2009.

444 Zaveri, R. A. and Peters, L. K.: A new lumped structure photochemical mechanism for large-scale applications, *J. Geophys.*
445 *Res.*, 104, D23, 30387–30415, <https://doi.org/10.1029/1999JD900876>, 1999.

446 Zaveri, R. A., Easter, R. C., Fast, J. D., and Peters, L. K.: Model for simulating aerosol interactions and chemistry (MOSA-
447 IC), *J. Geophys. Res.*, 113, D13204, <https://doi.org/10.1029/2007JD008782>, 2008.

448 Zeng, C., Liu, C., Li, J., Zhu, B., Yin, Y., and Wang, Y.: Optical Properties and Radiative Forcing of Aged BC due to Hygro-
449 scopic Growth: Effects of the Aggregate Structure, *J. Geophys. Res. Atmos.*, 124, 4620–4633,
450 <https://doi.org/10.1029/2018JD029809>, 2019.

451 Zhang, H., Chen, G., Hu, J., Chen, S. H., Wiedinmyer, C., Kleeman, M., & Ying, Q. Evaluation of a seven-year air quality
452 simulation using the Weather Research and Forecasting (WRF)/Community Multiscale Air Quality (CMAQ) models in
453 the eastern United States, *Sci. Total Environ.*, 473, 275-285, <https://doi.org/10.1016/j.scitotenv.2013.11.121>, 2014a.

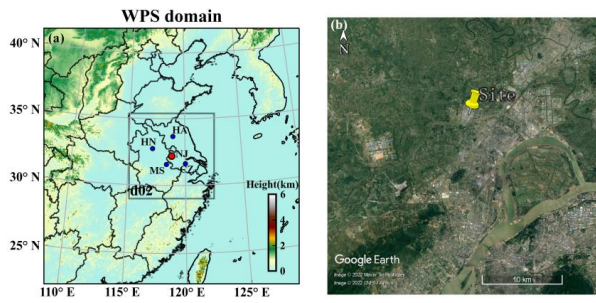
454 Zhang, H., DeNero, S. P., Joe, D. K., Lee, H.-H., Chen, S.-H., Michalakes, J., and Kleeman, M. J.: Development of a source
455 oriented version of the WRF/Chem model and its application to the California regional PM₁₀/PM_{2.5} air quality study,
456 *Atmos. Chem. Phys.*, 14, 485–503, <https://doi.org/10.5194/acp-14-485-2014>, 2014b.

457 Zhao, S., Hu, B., Liu, H., Du, C., Xia, X., & Wang, Y.: The influence of aerosols on the NO₂ photolysis rate in a suburban
458 site in North China, *Sci. Total Environ.*, 767, 144788, <https://doi.org/10.1016/j.scitotenv.2020.144788>, 2021.

459 Zheng, B., Tong, D., Li, M., Liu, F., Hong, C., Geng, G., Li, H., Li, X., and Peng, L.: Trends in China’s anthropogenic emis-
460 sions since 2010 as the consequence of clean air actions, *Atmos. Chem. Phys.*, 18, 14095–14111,
461 <https://doi.org/10.5194/acp-18-14095-2018>, 2018.

462 Zhu, B., Kang, H. Q., Zhu, T., Su, J. F., Hou, X. W., and Gao, J. H.: Impact of Shanghai urban land surface forcing on down-
463 stream city ozone chemistry, *J. Geophys. Res.-Atmos.*, 120, 4340–4351, <https://doi.org/10.1002/2014JD022859>, 2015.

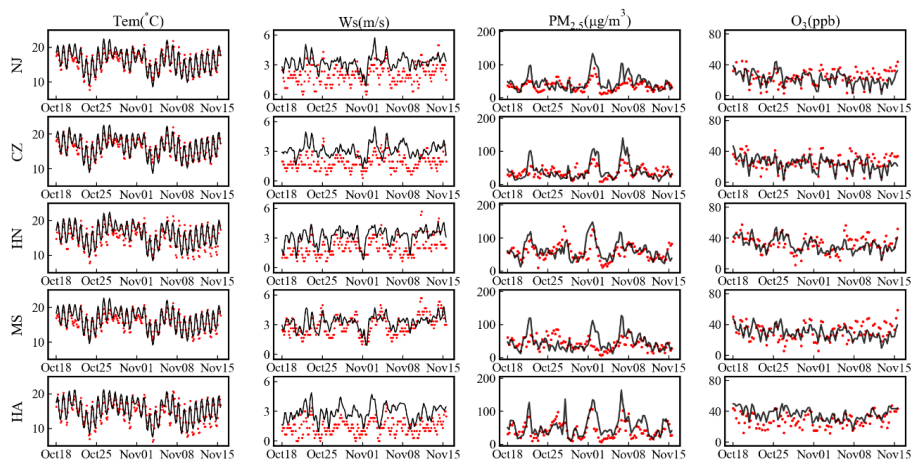
464



465

466 Figure 1. The model simulation domain (a) and the surrounding area of the observation site (b). The red point in (a)
 467 and the yellow symbol in (b) are the observation site in Nanjing (NJ). The four blue points in (a) are Changzhou (CZ),
 468 Huainan (HN), Maanshan (MS) and Huaian (HA) sites.

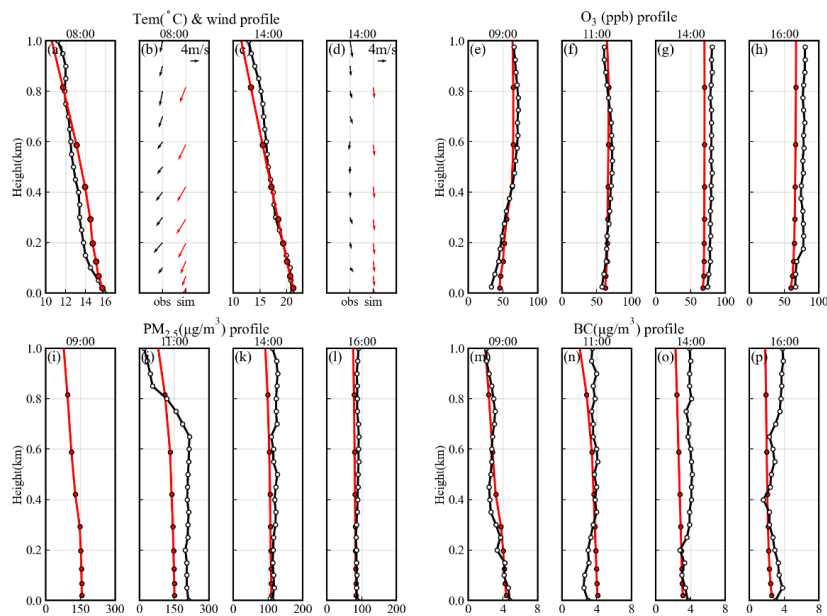
469



470

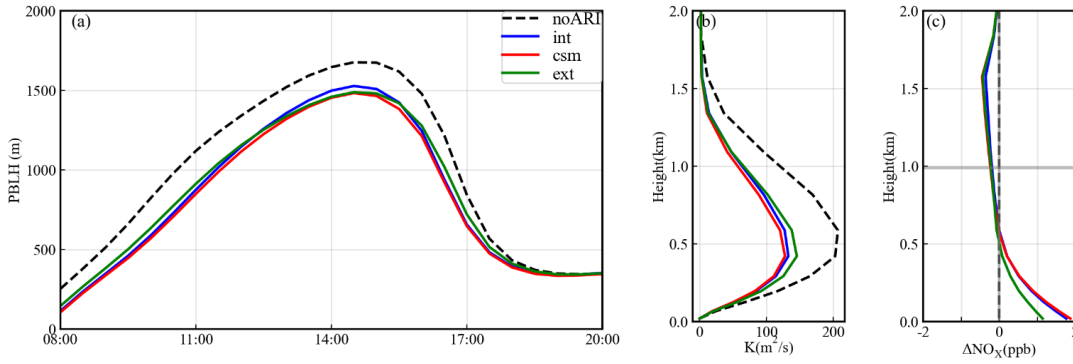
471 **Figure 2.** Model evaluations on the time series on temperature (Tem), wind speed (Ws), PM_{2.5} and Ozone at five sites.
 472 The Changzhou (CZ), Huainan (HN), Maanshan (MS) and Huaian (HA) sites are located to the east, west, south and
 473 north of Nanjing, respectively. The red dots are observations and black lines are simulations (after 3-point running av-
 474 erage). The time range is from 08:00 on 15 October to 20:00 on 15 November.

批注 [yansq10]: A newly added figure



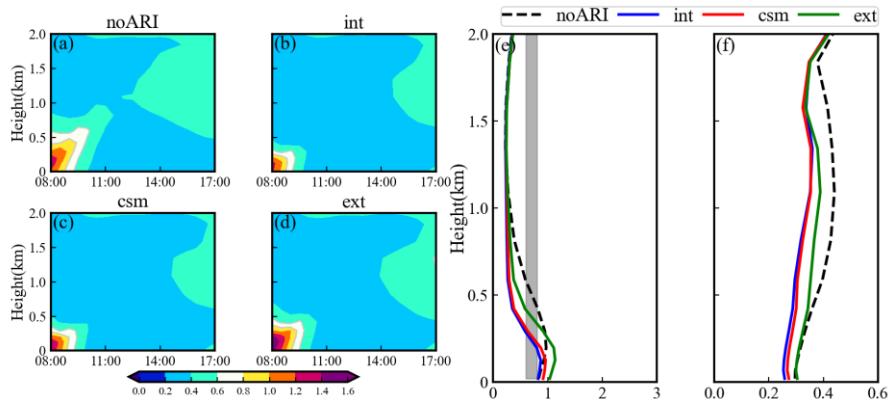
476

477 Figure 3. Model evaluations on the profiles of temperature, wind (vectors), ozone, PM_{2.5} and BC on 2 November
 478 2020. The black color is observation and the red color is simulation. The PM_{2.5} observation data at 09:00
 479 is missing due to instrument failure.



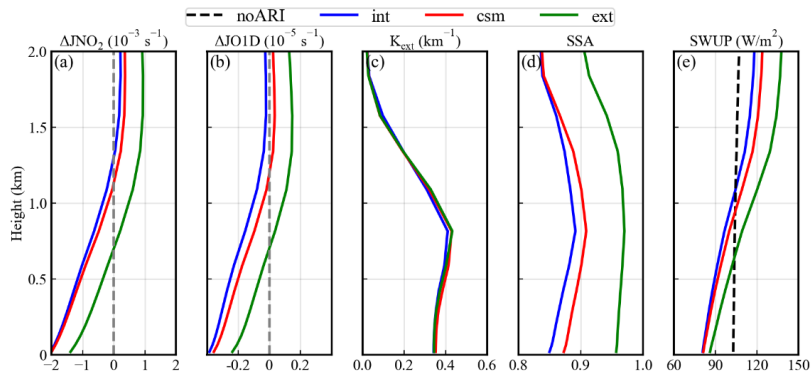
480

481 Figure 4. Time series of PBLH (a), profile of turbulent exchange coefficient K (b) and aerosol-induced change of
 482 NO_x profile (c) under different mixing states. The horizontal line in (c) is the PBLH of the base experiment. The pro-
 483 files and PBLH in (c) are averaged during 08:00~17:00.
 484



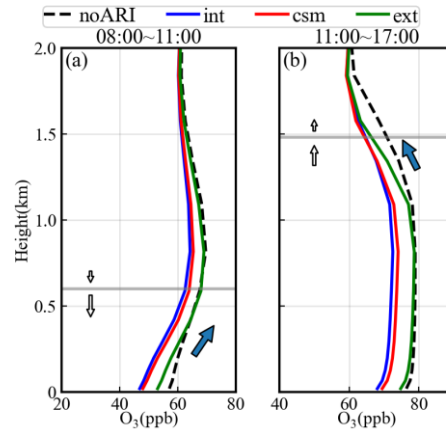
485

486 Figure 5. (a-d) Time-height distribution of ozone chemical regime (indicated by $R = \text{H}_2\text{O}_2/\text{HNO}_3$) in different aerosol
 487 mixing states. (e-f) Profiles of R averaged during 08:00~10:00 and 10:00~17:00, respectively. The white contours in
 488 (a-d) and the grey strips in (e-f) represent the transition regime ($0.6 < R < 0.8$).
 489



490

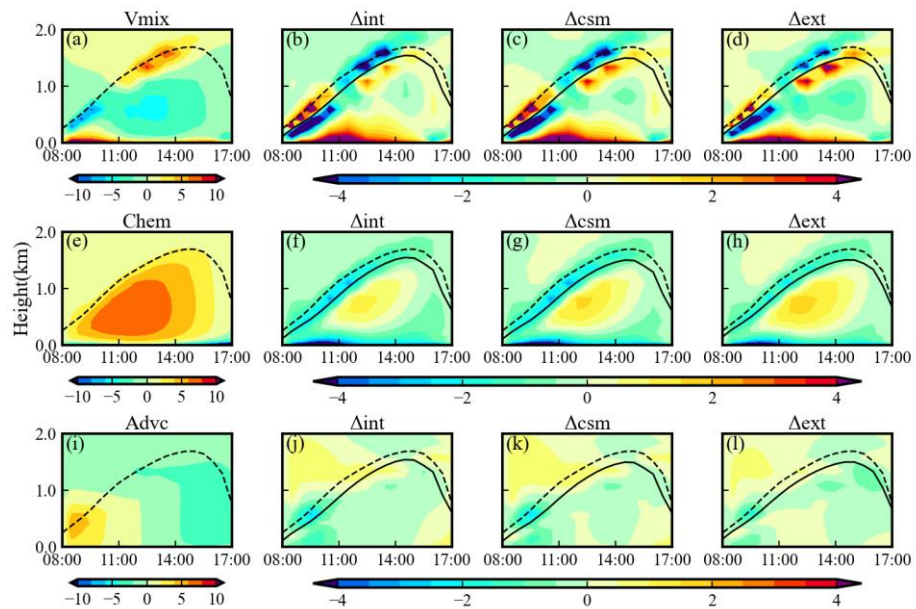
491 Figure 6. Comparisons of JNO_2 (a), $JO1D$ (b), aerosol extinction coefficient (c), single scatter albedo (d) and
 492 upwelling shortwave flux (e) profiles among different mixing states. For JNO_2 and $JO1D$, the profiles are the changes
 493 with respect to noARI condition. Profiles are time averages during 11:00~17:00.
 494



496

497 Figure 7. Ozone profiles under different mixing states. (a) 08:00~11:00 average. (b) 11:00~17:00 average. The hori-
 498 zontal line is PBLH. The blue arrows highlight the ozone vertical gradient at corresponding heights. The white arrows
 499 qualitatively describe the direction and magnitude of ozone turbulent exchange at the corresponding heights above or
 500 below PBLH.

501



502

503

504

505

506

Figure 8. The time-height distribution of process tendencies (ppb/h) that contribute to ozone variation. The three rows are Vmix, Chem and Advc, respectively. The first column is the ozone tendency in noARI condition, and the rest three columns are the changes in ozone tendency under different aerosol mixing states.

507 Table 1. Physical and chemical parameterization schemes.

Scheme	Option
Boundary layer	YSU
Microphysics	Lin
Longwave radiation	RRTMG
Shortwave radiation	RRTMG
Land surface	Noah
Grid nudging	On
Observation nudging	Off
Gas phase chemistry	CBMZ
Aerosol chemistry	MOSAIC-4bin
Aerosol-radiation feedback	On
Aerosol optical properties	Varies with experiments

508

509 Table 2. Settings of sensitive experiments.

Case name	Aerosol mixing states
int	internally mixed; base experiment
csm	core-shell mixed
ext	externally mixed
noARI	turn off aerosol-radiation feedback
Effect	Description
$\Delta_{\text{int}}=\text{int-noARI}$	effect by internal mixing
$\Delta_{\text{csm}}=\text{csm-noARI}$	effect by core-shell mixing
$\Delta_{\text{ext}}=\text{ext-noARI}$	effect by external mixing

510
511

512

513 Table 3. The **statistic metrics** of the model performance on time series of temperature (Tem), wind speed (WS), wind
 514 direction (WD), PM_{2.5} and ozone. The benchmark values are from Emery et al. (2011) and EPA (2005; 2007). Metrics
 515 that out of benchmarks are marked with red. (Nanjing:NJ, Changzhou:CZ, Huainan:HN, Maanshan:MS, Huaian:HA)

Variable	Metric	NJ	CZ	HN	MS	HA	benchmark
Tem	IOA	0.97	0.97	0.96	0.97	0.96	>0.8
	MB	0.18	0.18	0.42	0.31	0.50	<±0.5
	RMSE	1.07	1.07	1.43	1.10	1.52	
WS	IOA	0.64	0.63	0.66	0.71	0.64	>0.6
	MB	0.47	0.68	0.52	-0.05	0.71	<±0.5
	RMSE	1.13	1.06	1.09	0.88	1.09	<2
WD	IOA	0.94	0.93	0.93	0.95	0.88	
	MB	-3.32	10.47	9.91	-4.65	6.16	<±10
	RMSE	35.91	38.53	46.31	36.56	52.92	
PM _{2.5}	IOA	0.74	0.84	0.83	0.64	0.86	
	MNB	0.26	0.01	0.12	0.36	0.34	
	MFB	0.17	-0.04	0.06	0.23	0.22	<±0.6
Ozone	IOA	0.87	0.88	0.91	0.83	0.88	
	MNB	-0.07	-0.03	0.03	0.03	0.20	<±0.15
	MFB	-0.15	-0.07	0.02	0.03	0.17	

批注 [y11]: A new table is added

516

517

518

519

520

521
522
523

~~Table 4. The contribution of aerosol to ozone process tendencies (ppb/h) under different mixing states during 11:00–17:00. The values are averaged below the PBLH. The parentheses are relative contributions of each process, e.g., $\Delta_{\text{mix}}/(|\Delta_{\text{mix}}| + |\Delta_{\text{chem}}| + |\Delta_{\text{adv}}|) * 100\%$.~~

批注 [yansq12]: The table is deleted.

	int	esm	ext
H: 0–300m			
Δ_{mix}	+2.9 (+53.2%)	+2.8 (+53.7%)	+2.3 (+57.4%)
Δ_{chem}	-2.2 (-39.5%)	-2.0 (-38.7%)	-1.5 (-37.3%)
Δ_{adv}	+0.4 (+7.4%)	+0.4 (+7.5%)	+0.2 (+5.4%)
H: 300–800m			
Δ_{mix}	+0.0 (+3.0%)	-0.2 (+13.2%)	-0.4 (-25.1%)
Δ_{chem}	+0.5 (+52.6%)	+0.5 (+57.6%)	+0.8 (+65.8%)
Δ_{adv}	+0.4 (+44.4%)	+0.4 (+29.1%)	+0.2 (+9.2%)
H: 800–1500m			
Δ_{mix}	-1.5 (+71.9%)	+2.0 (+79.0%)	+1.4 (+65.5%)
Δ_{chem}	+0.1 (+3.1%)	-0.0 (-0.3%)	+0.6 (+28.2%)
Δ_{adv}	+0.5 (+25.1%)	+0.5 (+20.7%)	+0.1 (+6.3%)

524

525
526

Table 5. The diurnal averaged (08:00–17:00) variations of ozone, NO_x and JNO₂ variations caused by different aerosol mixing states in urban and rural conditions. The statistics are conducted at the entire model grids.

	Δ_{int}	Δ_{csm}	Δ_{ext}
$\Delta Ozone$ (ppb) (0.0–1.5km)			
urban	-6.4(-9.4%)	-4.9(-7.2%)	-0.4(-0.6%)
rural	-6.7(-10.1%)	-5.1(-7.8%)	-0.4(-0.6%)
ΔNO_x (ppb) (0.0–1.5km)			
urban	+0.8(+17.2%)	+0.8(+15.3%)	+0.3(+6.8%)
rural	+0.6(+20.4%)	+0.5(+17.7%)	+0.2(+6.2%)
ΔJNO_2 ($10^{-3}s^{-1}$) (0.0–1.0km)			
urban	-0.9(-16.8%)	-0.8(-14.5%)	-0.2(-3.9%)
rural	-1.0(-17.1%)	-0.9(-14.7%)	-0.2(-3.7%)
ΔJNO_2 ($10^{-3}s^{-1}$) (1.0–1.5km)			
urban	+0.1(+2.0%)	+0.3(+4.9%)	+1.0(+14.3%)
rural	+0.1(+1.2%)	+0.3(+4.4%)	+1.1(+14.9%)

批注 [yansq13]: The original version of Table 4

527

Table 4. The diurnal averaged (08:00~17:00) variations of ozone, NO_x and JNO₂ variations caused by different aerosol mixing states at four sites around Nanjing, urban areas and rural areas. The urban (rural) means the averages over urban (rural) surfaces of the model grids. The date is 2 November 2020. (Changzhou:CZ, Huainan:HN, Maanshan:MS, Huaian:HA)

	CZ	HN	MS	HA	urban	rural
$\Delta Ozone$ (ppb) (0.0~1.5km)						
Δ_{int}	-8.8(-12.1%)	-3.5(-5.8%)	-6.0(-8.3%)	-5.8(-8.7%)	-5.3(-8.5%)	-5.0(-7.9%)
Δ_{csm}	-8.1(-11.1%)	-3.1(-5.1%)	-4.8(-6.7%)	-5.0(-7.4%)	-4.4(-7.1%)	-4.2(-6.7%)
Δ_{ext}	-3.7(-5.1%)	-1.2(-2.0%)	-0.8(-1.0%)	-1.4(-2.1%)	-1.1(-1.8%)	-0.9(-1.5%)
ΔNO_x (ppb) (0.0~1.5km)						
Δ_{int}	0.7(+16.2%)	0.6(+20.7%)	0.6(+12.3%)	0.4(+20.6%)	0.7(+11.4%)	0.5(+16.2%)
Δ_{csm}	0.7(+16.8%)	0.7(+22.3%)	0.5(+11.3%)	0.4(+20.9%)	0.7(+10.3%)	0.5(+15.0%)
Δ_{ext}	0.6(+14.3%)	0.5(+15.5%)	0.2(+3.4%)	0.2(+10.2%)	0.3(+5.0%)	0.2(+6.3%)
ΔJNO_2 ($10^{-3}s^{-1}$) (0.0~1.0km)						
Δ_{int}	-1.4(-25.7%)	-1.0(-16.1%)	-1.5(-23.1%)	-1.3(-21.0%)	-0.9(-18.7%)	-1.1(-18.6%)
Δ_{csm}	-1.4(-24.6%)	-1.0(-15.5%)	-1.4(-21.9%)	-1.3(-20.4%)	-0.8(-17.3%)	-1.0(-17.4%)
Δ_{ext}	-0.9(-15.9%)	-0.5(-7.1%)	-0.7(-11.1%)	-0.7(-10.6%)	-0.4(-7.6%)	-0.4(-7.3%)
ΔJNO_2 ($10^{-3}s^{-1}$) (1.0~1.5km)						
Δ_{int}	-0.0(-0.5%)	-0.0(-0.2%)	-0.1(-1.7%)	-0.1(-1.8%)	-0.2(-3.5%)	-0.1(-1.4%)
Δ_{csm}	0.2(+2.3%)	0.0(+0.5%)	0.0(+0.7%)	-0.0(-0.5%)	-0.1(-1.7%)	0.0(+0.4%)
Δ_{ext}	0.7(+9.4%)	0.5(+7.5%)	0.7(+9.7%)	0.6(+8.2%)	0.4(+6.4%)	0.7(+9.3%)

批注 [yansq14]: The original Table4 is changed: the statistical values at more sites are presented.

532

533

534 Table 5. The diurnal averaged (08:00~17:00) quantities within BL during some representative clean and polluted epi-
 535 sodes. The $PM_{2.5}$ ($\mu\text{g}/\text{m}^3$) and ozone (ppb) are the values in the internal mixing state. The last three columns are the
 536 changes and relative changes of ozone under different mixing states.

Date	$PM_{2.5}$	Ozone	Δ_{int}	Δ_{csm}	Δ_{ext}
Clean episode					
10-19	32	53	-1.9 (-3.5%)	-1.7 (-3.1%)	+0.0 (+0.0%)
10-20	18	49	-0.8 (-1.5%)	-0.7 (-1.4%)	+0.1 (+0.1%)
10-25	28	53	-2.0 (-3.6%)	-1.9 (-3.5%)	-0.2 (-0.3%)
11-03	33	39	-0.7 (-1.8%)	-0.7 (-1.8%)	-0.4 (-1.1%)
11-05	17	44	-1.5 (-3.3%)	-1.5 (-3.3%)	-0.9 (-1.9%)
11-12	23	36	-1.9 (-4.9%)	-1.9 (-4.9%)	-0.9 (-2.5%)
Polluted episode					
10-22	91	46	-3.0 (-6.1%)	-2.8 (-5.6%)	-0.3 (-0.7%)
11-02	111	56	-7.7 (-10.5%)	-6.4 (-8.6%)	-1.5 (-2.0%)
11-07	87	39	-4.6 (-10.7%)	-4.6 (-10.6%)	-1.6 (-3.7%)
11-08	82	39	-3.0 (-7.0%)	-2.8 (-6.6%)	-0.6 (-1.4%)

537

538

539

540